RSC Advances

ROYAL SOCIETY OF CHEMISTRY

www.rsc.org/advances

Journal Name

COMMUNICATION

Facile synthesis of uniform yolk-shell structured magnetic mesoporous silica as an advanced photo-Fenton-like catalyst for degrading rhodamine B

Received 00th January 20xx,
Accepted 00th January 20xx

DOI: 10.1039/x0xx00000x

www.rsc.org/

Pengpeng Qiu,[a‡] Kyounglim Kang,[a, b‡] Kyungho Kim,[a] Wei Li,[c] Mingcan Cui,[a] and Jeehyeong Khim[*a]

Through an ultrasound assisted etching method, uniform yolk–shell structured magnetic mesoporous silica (Fe_3O_4@void@$mSiO_2$) nanosphere has been fabricated and for the first time demonstrated as an efficient catalyst for degrading rhodamine B under photo-Fenton-like condition.

Fenton reaction based on ferrous ions and hydrogen peroxide has been widely investigated as an effective way to degrade organic pollutants through the hydroxyl radical oxidation. However, the narrow working pH range (< 4), difficulties to recover the dissolved metal ions and necessity for further treatment of ferric hydroxide sludge greatly hinder its wide application for practical water treatment.[1] To this end, synthesis of a magnetically separable Fenton-like catalyst is highly desired.[2] More importantly, magnetite nanoparticles (NPs) has been extensively demonstrated as the most effective heterogeneous Fenton catalyst among Fe-based materials as it contains higher content of structural Fe^{2+}.[3] However, Fe_3O_4 NPs still have some shortcomings such as spontaneous aggregation due to high surface energy, limited adsorption ability owing to its low surface area and small pore volume, readily contaminated catalytic sites when exposed to bulk solution and relevant low H_2O_2 activation activity because of the fully oxidized surface.[4] Therefore, immobilizing Fenton catalysts into a porous matrix and irradiation with UV light has been regarded as an ideal way to address the above difficulties.[5]

Recently, yolk−shell structured materials with a typical core@void@shell architecture have received considerable attention. With the appealing structures of movable cores, interstitial hollow spaces and multifunctional shells, this kind of material holds an important role in modern science and technology as potential candidates for tremendous applications such as confined catalysis,[6] lithium-ion batteries,[7] drug delivery,[8] and sensors[9]. Among them, the Fe_3O_4@void@mesoporous SiO_2 ($mSiO_2$) nanostructures are of great interest and importance owing to their multifunctional properties including abundant catalytic sites, strong magnetic separation ability, and excellent biocompatibility and versatility in surface functionalization as well as the high surface area, ordered mesoporous structure and large porosity of $mSiO_2$ greatly facilitating guest molecule adsorption and diffusion.[10] To date, substantial research efforts have been made to synthesis of this type of material. One common strategy involves the use of polymeric carbon interlayer as a hard template, which can be selectively removed by calcination or solvent extraction, for the formation of yolk-shell structures.[6a,11] However, this strategy is often associated with some disadvantages such as requiring high energy cost, producing materials with collapsed mesoporous structures, etc.[12] To solve these problems, an alternative method termed as "surface protected etching approach" has been developed to synthesize high-quality yolk-shell/hollow structured silica materials. Solid silica spheres or a silica interlayer was used as templates to create desired structures with the protection of some polymeric ligands or templates.[8b, 13] However, the investigation of yolk-shell structured magnetic mesoporous silica as a photo-Fenton-like catalyst has rarely been reported so far.

Herein, we report an ultrasound assisted etching method to synthesize uniform yolk-shell structured magnetic mesoporous silica nanospheres consisting of a movable magnetite core, interstitial void spaces and a mesoporous silica shell. This etching strategy is facile, mild and effective. The resultant material has been demonstrated as a catalyst in the photo-Fenton-like process, showing a remarkable degradation performance for rhodamine B (RhB) in a wide range of pH values (3 – 7). More importantly, the catalysts can be easily recycled within a short time (< 2 min) by using an external magnetic field and a constant catalytic activity is retained even after five cycles. This study paves a promising way for the design and synthesis of multifunctional catalyst for the photo-Fenton like process.

[a] *School of Civil Environmental and Architecture Engineering, Korea University, Seoul 136-701, Republic of Korea. E-mail:* hyeong@korea.ac.kr
[b] *Department of Environmental Geosciences, University of Vienna, 1010 Vienna, Austria.*
Laboratory of Advanced Materials and Department of Chemistry, Fudan University, Shanghai 200433, China.
‡ *The contribution is equal.*

†Electronic Supplementary Information (ESI) available: [details of any supplementary information available should be included here]. See DOI: 10.1039/x0xx00000x

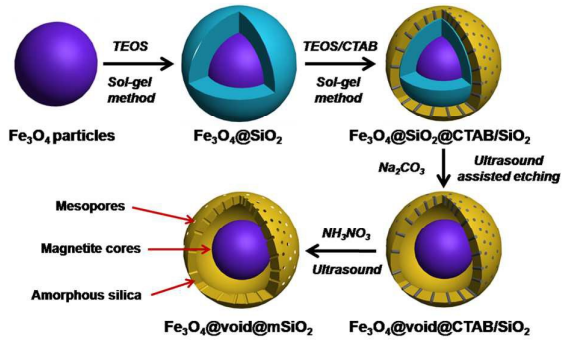

Fig. 1 Schematic illustration for the synthesis of the yolk-shell structured Fe_3O_4@void@mSiO_2 nanospheres *via* an ultrasound assisted etching method.

The synthesis strategy for the yolk-shell structured magnetic mesoporous silica nanospheres is depicted in Fig. 1. First, the uniform magnetite particles were coated with a nonporous silica layer through a sol-gel approach in the presence of tetraethyl orthosilicate (TEOS) (denoted as Fe_3O_4@SiO_2).[14] Then, a further sol-gel coating process was utilized to deposit a mesoporous silica shell onto the nonporous silica layer with the help of a cationic template hexadecyl trimethyl ammonium bromide (CTAB) (defined as Fe_3O_4@SiO_2@mSiO_2). Finally, an ultrasound assisted etching method was used to etch off the nonporous silica layer in a weak alkaline media, after which the CTAB was removed in an ammonia nitrate ethanol solution, leading to the resultant yolk-shell structured magnetic mesoporous silica nanospheres (designated as Fe_3O_4@void@mSiO_2).

The scan electron microscopy (SEM) images reveal that the obtained Fe_3O_4 particles possess a uniform spherical shape with an average diameter of ~ 130 nm (Fig. S1A and B). After the first sol-gel coating process, transmission electron microscopy (TEM) images clearly show that a nonporous silica layer with a thickness of ~ 30 nm is uniformly coated onto the magnetic cores, resulting in a well-defined core-shell structure (Fig. S1C and D). A subsequent sol-gel coating process leads to the deposition of a mesoporous silica shell onto the surface of Fe_3O_4@SiO_2 nanospheres. TEM images (Fig. 2A and B) clearly depict that Fe_3O_4@SiO_2@mSiO_2 nanospheres possess a typical sandwich-like core–shell-shell structure with an outer mesoporous silica shell (~ 30 nm). After the ultrasound assisted etching and extracting processes, a well-defined yolk-shell nanostructure with perpendicular mesopores (~2.8 nm) is obtained (Fig. 2C and D). The spacing between the inner magnetite cores and the outer mesoporous silica shells is measured to be ~ 30 nm, well corresponding to the thickness of the nonporous silica layer, suggesting that the condensed silica layer can be selectively removed in Na_2CO_3 solution under ultrasound irradiation. The template CTAB served as a "surface protecting agent", greatly increasing the stability of outer mesoporous silica shell against etching. [15] In contrast, it is hard to get unambiguous yolk-shell structures under the conditions without ultrasound, even extending the reaction time to 12 h (Fig. S2). However, when ultrasonic irradiation was used, uniform yolk-shell structure can be obtained in a very short aging time (6 h). This can be attributed to that the high-speed microjects (100 ms^{-1}) and enormous localized temperature (5000 K) generated from cavitation bubbles collapse greatly accelerate the diffusion and etching process.[16] Moreover, hollow mesoporous silica (H-mSiO_2) can be obtained by etching off the inner magnetite cores with HCl solution (Fig.S3).

N_2 sorption isotherms of the yolk-shell structured magnetic mesoporous silica nanospheres (Fig. 3A) show a characteristic IV curve with a hysteresis loops close to H_1-type and an increase in the adsorption branch at a relative pressure of P/P_0 = 0.2 ~ 0.5, further suggesting that the outer silica shells contain uniform mesopores. In addition, the loop with parallel branches at the relative pressure between 0.1 and 0.4 is attributed to the cavity between the magnetic core and the outer shell.[17] The BET surface area and pore volume of the Fe_3O_4@void@mSiO_2 nanospheres are measured to be 406.1 m^2 g^{-1} and 0.34 cm^3 g^{-1}, respectively. Correspondingly, the pore size distribution (Fig. 3 B) calculated from the adsorption branch using the Barrett-Joyner-Halenda (BJH) method reveals a uniform pore

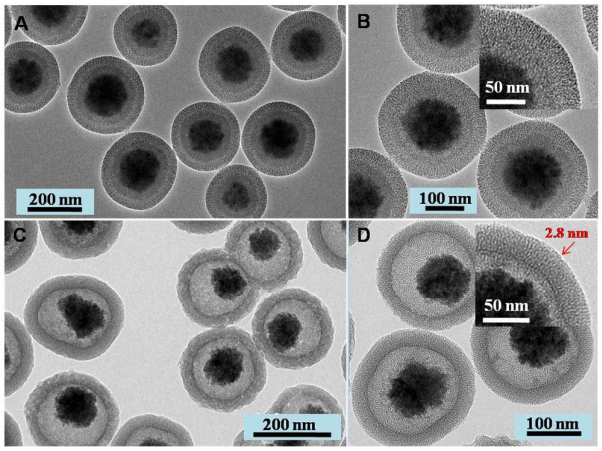

Fig.2 TEM images of the Fe_3O_4@SiO_2@mSiO_2 nanospheres (A and B) synthesized through two-steps sol-gel method and Fe_3O_4@void@mSiO_2 nanospheres (C and D) fabricated *via* an ultrasound assisted etching method.

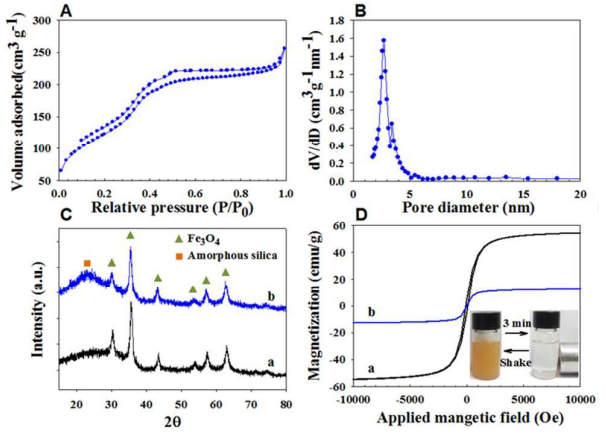

Fig.3 (A) N_2 sorption isotherms and (B) pore-size distributions of the Fe_3O_4@void@mSiO_2 nanospheres; (C) XRD patterns of (a) the Fe_3O_4 particles and (b) uniform yolk-shell structured Fe_3O_4@void@mSiO_2 nanospheres and (D) The magnetic hysteresis loops at 300 K of (a) Fe_3O_4 spheres and (b) uniform yolk-shell structured Fe_3O_4@void@mSiO_2 nanospheres. Inset shows the simple magnetic separation process *via* a hand-held magnet

size centered at ~ 2.8 nm, which is similar to the TEM results. The X-ray diffraction pattern (XRD) of the Fe_3O_4@void@$mSiO_2$ nanospheres (Fig. 3C) shows six well resolved characteristic diffraction peaks, which are typical for Fe_3O_4 crystalline phase. In addition, a broad amorphous silica peak can be clearly distinguished compared with XRD pattern of pure Fe_3O_4 NPs. The magnetization saturation values of pristine Fe_3O_4 and Fe_3O_4@void@$mSiO_2$ nanospheres are measured to be ~ 58.4 and 18 emu/g, respectively (Fig. 3D). As a result of the superparamagnetic property and high magnetization, the Fe_3O_4@void@$mSiO_2$ nanospheres in their homogeneous dispersion show fast motion under the applied magnetic field and quick dispersibility upon a slight shake when the magnetic field is removed (Fig. 3D insert).

The performance of the resultant magnetic mesoporous silica on the photo-Fenton-like catalytic degradation of RhB was examined at pH 3 (Fig. 4A). As a control, the degradation performances of RhB under H_2O_2, UV/H_2O_2, and Fe_3O_4@void@$mSiO_2$/H_2O_2 condition were also tested, exhibiting the removal efficiencies of 5.0, 39.5, and 25.5 %, respectively. The higher degradation efficiency of UV/H_2O_2 process was due to the decomposition of H_2O_2 into hydroxyl radicals through UV light (UVA is not able to decompose RhB molecules).[17] However, when Fe_3O_4@void@$mSiO_2$ nanospheres were used as a Fenton catalyst without UV light, the efficiency was not significant compared with the adsorption efficiency of Fe_3O_4@void@$mSiO_2$ (18.7 %, Fig. 4B), which might result from the fully oxidized Fe_3O_4 surface inhibiting the activation of H_2O_2. Interestingly, when combine UV, H_2O_2 and Fe_3O_4@void@$mSiO_2$ catalyst together, the degradation performance of RhB was greatly improved and 98.3% degradation of RhB was observed in 160 min, indicating the importance of irradiation of UV light. This is because the irradiation of light can not only initiate the Fenton reaction by recovering the surface Fe^{3+} into Fe^{2+} based on light induced electron transfer according to the Haber-Weiss mechanism, but also prevent self recombination of hydroxyl radical by rapidly decomposing H_2O_2 into hydroxyl radical, thus increasing the utilization efficiency of H_2O_2 and Fe^{2+}.[19] To demonstrate the priority of Fe_3O_4@void@$mSiO_2$ nanospheres, the degradation performances of magnetite and H-$mSiO_2$ under photo-Fenton condition were also tested. Clearly, the degradation efficiencies of magnetite and H-$mSiO_2$ are 82.0 and 55 %, respectively, which are much smaller than that of Fe_3O_4@void@$mSiO_2$ catalyst. The remarkable performance of the magnetic mesoporous silica can be attributed to the synergistic effect from its unique textual structures, as illustrated in Fig. 4C. First, the large pore size (~ 2.8 nm) and ordered mesopores favored the mass transfer of both H_2O_2 and RhB (1.5 × 0.43 × 0.98 nm) molecules between aqueous and solid phases. Second, the presence of mesoporous silica shell can greatly enhance the adsorption of RhB molecules and enrich them in the void space of the nanoreactor,[20] which would be beneficial for surface hydroxyl radical oxidation rate. The adsorption test (Fig. 4B) clearly shows that the magnetic mesoporous silica possesses a 2 times higher adsorption efficiency than that of Fe_3O_4 (8.5 %). Finally, the recovered Fe^{2+} reacts with the adsorbed H_2O_2 to produce large amount of hydroxyl radicals. These hydroxyl radicals can directly in-situ oxidize the RhB molecules confined in the void space into small molecules or even CO_2 and H_2O, thus lowering the self recombination reaction rate of •OH that usually occurs in the oxidation process within the bulk

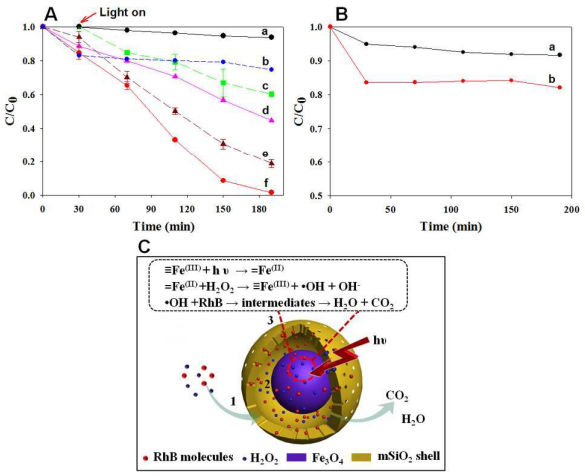

Fig.4. (A) The photo-Fenton catalytic degradation performance of RhB under varied conditions: (a) H_2O_2 alone, (b) Fe_3O_4@void@$mSiO_2$/H_2O_2 process, (c) UV/H_2O_2 process, (d) UV/$mSiO_2$/H_2O_2 process, (e) UV/Fe_3O_4/H_2O_2, and (f) UV/Fe_3O_4@void@$mSiO_2$/H_2O_2. Before initiation of the reaction, the mixture was mechanically stirred in dark for 30 min to reach the adsorption/desorption equilibrium between the catalyst and pollutants, (B) The adsorption test of (a) Fe_3O_4 NPs and (b) Fe_3O_4@void@$mSiO_2$ nanospheres. Other factors were controlled as constants: pH = 3, T = 25 ºC, and stirring speed = 300 rpm, and (C) Schematic illustration for the photo-Fenton catalytic degradation of RhB in the presence of yolk-shell structured magnetic mesoporous silica spheres: (1) Enhanced mass transfer by large ordered mesopores; (2) Enrichment of H_2O_2 and RhB molecules within the void space; (3) Surface recovery and in-situ oxidation of organic pollutant on Fe_3O_4 particles.

phase. The effect of pH on the degradation performance of Fe_3O_4@void@$mSiO_2$ (Fig. S4A) was investigated. We found that the removal efficiency at pH = 6.2 is still 88.0 %, suggesting that such catalysts can work in a neutral pH. However, when the pH was extended to 10, the efficiency sharply decreased, which is possibly due to the self decomposition of H_2O_2 into water and oxygen.[21] The recycle test of the yolk-shell structured Fe_3O_4@void@$mSiO_2$ at pH 3 was examined (Fig. S4B). After five recycles, a constant degradation performance was retained, indicating the excellent reusability of this material. As a comparison, the recycle test of Fe_3O_4 was also tested. Notably, the removal efficiency of RhB decreased from 82.0% to 71.0% (13.4% loss) after recycling five times (Fig.S4B.b). The poor reusability of Fe_3O_4 can be attributed to the high total Fe leaching rate and rapid weight loss during recycling (Fig. S5).

In summary, we report the synthesis of uniform yolk-shell structured magnetic mesoporous silica nanospheres *via* a straightforward route. An ultrasound assisted etching method was first demonstrated to selectively remove the nonporous silica layer, which is facile, mild and effective. The resultant Fe_3O_4@void@$mSiO_2$ nanospheres possess uniform mesopores (~ 2.8 nm), a high BET surface area (~ 406.1 m^2 g^{-1}) and a large pore volume (~ 0.34 cm^3 g^{-1}) as well as a high magnetic susceptibility (~ 18.0 emu g^{-1}). Then, it was demonstrated as an advanced photo-Fenton-like catalyst, showing a remarkable performance for degrading RhB. Moreover, the catalyst can work in a wide pH range (3 – 7) and exhibit an excellent reusability. This study paves a great

way to synthesize and design a multifunctional material for the photo-Fenton like process.

We thank the National Natural Science Foundation of China (21471034) and National Research Foundation of Korea (NRF, 2013R1A1A2006586) for financial support.

Notes and references

1 (a) E. Neyens and J. Baeyens, *J. Hazard. Mater*., 2003, **98**, 33-50; (b) S. Caudo, G. Centi, C. Genovese and S. Perathoner, *Top. Catal*., 2006, **40**, 207-219.

2 (a) Y. Wang, H. Zhao, M. Li, J. Fan and G. Zhao, *Appl. Catal., B: Environ*., 2014, **147**, 534-545; (b) K. Rusevova, F. D. Kopinke and A. Georgi, *J. Hazard. Mater*., 2012, **241–242**, 433-440; (c) L. Xu and J. Wang, *Environ. Sci. Technol*., 2012, **46**, 10145-10153.

3 (a) J. He, X. Yang, B. Men, Z. Bi, Y. Pu and D. Wang, *Chem. Eng. J*., 2014, **258**, 433-441; (b) R. Guo, L. Fang, W. Dong, F. Zheng and M. Shen, *J. Mater. Chem*., 2011, **21**, 18645-18652.

4 (a) P. Avetta, A. Pensato, M. Minella, M. Malandrino, V. Maurino, C. Minero, K. Hanna and D. Vione, *Environ. Sci. Technol*., 2015, **49**, 1043-1050; (b) S. T. Yang, W. Zhang, J. Xie, R. Liao, X. Zhang, B. Yu, R. Wu, X. Liu, H. Li and Z. Guo, *RSC Adv*., 2015, **5**, 5458-5463.

5 (a) M. B. Kasiri, H. Aleboyeh and A. Aleboyeh, *Appl. Catal., B: Environ*., 2008, **84**, 9-15; (b) Y. Ling, M. Long, P. Hu, Y. Chen and J. Huang, *J. Hazard. Mater*., 2014, **264**, 195-202.

6 (a) Z. M. Cui, Z. Chen, C. Y. Cao, L. Jiang and W.G. Song, *Chem. Commun*., 2013, **49**, 2332-2334; (b) T. Zeng, X. Zhang, S. Wang, Y. Ma, H. Niu and Y. Cai, *Chem. Eur. J*., 2014, **20**, 6474-6481; (c) C. Liu, J. Li, J. Qi, J. Wang, R. Luo, J. Shen, X. Sun, W. Han, and L. Wang, *ACS Appl. Mater. Interfaces*., 2014, **6**, 13167-13173.

7 (a) J. Wang, W. Li, F. Wang, Y. Xia, A. M. Asiri and D. Zhao, *Nanoscale*, 2014, **6**, 3217-3222; (b) W. Zhou, Y. Yu, H. Chen, F. J. DiSalvo and H. D. Abruña, *J. Am. Chem. Soc*., 2013, **135**, 16736-16743.

8 (a) J. Liu, S. Z. Qiao, S. Budi Hartono and G. Q. Lu, *Angew. Chem. Int. Ed*., 2010, **49**, 4981-4985; (b) Y. Chen, H. Chen, L. Guo, Q. He, F. Chen, J. Zhou, J. Feng and J. Shi, *ACS Nano*, 2010, **4**, 529-539; (c) J. Yang, D. Shen, L. Zhou, W. Li, X. Li, C. Yao, R. Wang, A. M. EI-Toni, F. Zhang and D. Zhao, *Chem. Mater*., 2013, 25, 3030-3037.

9 P. Rai, J. W. Yoon, H. M. Jeong, S. J. Hwang, C. H. Kwak and J.H. Lee, *Nanoscale*, 2014, **6**, 8292-8299.

10 (a) T. Yao, T. Cui, X. Fang, F. Cui and J. Wu, *Nanoscale*, 2013, **5**, 5896-5904; (b) W. Li and D. Zhao, *Adv. Mater*., 2013, **25**, 142-149.

11 W. Li, Q. Yue, Y. Deng and D. Zhao, *Adv. Mater*., 2013, **25**, 5129-5152.

12. J. Liu, S. Z. Qiao, J. S. Chen, X. W. Lou, X. Xing and G. Q. Lu, *Chem. Commun*., 2011, **47**, 12578-12591.

13 Q. Zhang, T. Zhang, J. Ge and Y. Yin, *Nano Lett*., 2008, **8**, 2867-2871.

14 (a) J. Liu, Z. Sun, Y. Deng, Y. Zou, C. Li, X. Guo, L. Xiong, Y. Gao, F. Li and D. Zhao, *Angew. Chem. Int. Ed*., 2009, **48**, 5875-5879; (b) W. Li, Y. Deng, Z. Wu, X. Qian, J. Yang, Y. Wang, D. Gu, F. Zhang, B. Tu and D. Zhao, *J. Am. Chem. Soc*., 2011, **133**, 15830-15833.

15 X. L. Fang, C. Chen, Z. H. Liu, P. X. Liu and N. F. Zheng, *Nanoscale*, 2011, **3**, 1632-1639.

16 (a) V. G. Pol, R. Reisfeld and A. Gedanken, *Chem. Mater*., 2002, **14**, 3920-3924; (b) P. Qiu, W. Li, K. Kang, B. Park, W. Luo, D. Zhao and J. Khim, *J. Mater. Chem. A*, 2014, **2**, 16452-16458; (c) A. Gedanken, X. Tang, Y. Wang, N. Perkas, Y. Koltypin, M. V. Landau, L. Vradman and M. Herskowitz, *Chem. Eur. J*., 2001, **7**, 4546-4552.

17 J. Liu, J. Cheng, R. Che, J. Xu, M. Liu and Z. Liu, *ACS Appl. Mater. Interfaces*, 2013, **5**, 2503-2509.

18 T. Aarthi and G. Madras, *Ind. Eng. Chem. Res*., 2007, **46**, 7-14.

19 J. Ndounla, S. Kenfack, J. Wéthé and C. Pulgarin, *Appl. Catal. B: Environ*., 2014, **148–149**, 144-153.

20 (a) B. Li, F. Li, S. Bai, Z. Wang, L. Sun, Q. Yang and C. Li, *Energy Environ. Sci*., 2012, **5**, 8229-8233; (b) S. Zhang, W. Xu, M. Zeng, J. Li, J. Li, J. Xu and X. Wang, *J. Mater. Chem. A*, 2013, **1**, 11691-11697; (c) C. X. Gui, Q. J. Li, L. L. Lv, J. Qu, Q. Q. Wang, S. M. Hao and Z. Z. Yu, *RSC Adv.*, 2015, **5**, 20440-20445.

21 Z. Qiang, J. H. Chang and C.P. Huang, *Water Res*., 2002, **36**, 85-94.

